High-Temperature, Short-Time Sulfation of Calcium-Based Sorbents. 1. Theoretical Sulfation Model

Corey R. Milne, Geoffrey D. Silcox,* and David W. Pershing
Department of Chemical Engineering, The University of Utah, Salt Lake City, Utah 84112

David A. Kirchgessner
Air and Energy Engineering Research Laboratory, U.S. Environmental Protection Agency, Research Triangle Park, North Carolina 27711

A mathematical model for the sulfation of CaO is developed around the overlapping grain concept. The potential influence of high mass-transfer rates from simultaneous calcination of $CaCO_3$ or $Ca(OH)_2$ is incorporated in the mass-transfer coefficient for SO_2 diffusion to the particle. A solution scheme for the nonlinear differential equation governing pore diffusion with changing particle structure is developed. The influence of grain overlap on product-layer diffusion is quantified. The model predictions show good agreement with published, fundamental differential reactor data which include the influences of surface area, temperature, and SO_2 partial pressure.

Introduction

Inspired by the necessity of reducing the level of acid rain precursors from coal-fired utility boilers, fundamental studies of the sulfation of CaO with SO_2

$$CaO(s) + SO_2(g) + \tfrac{1}{2}O_2(g) \rightarrow CaSO_4(s) \qquad (1)$$

have been prevalent since the early 1970s. What once may have seemed a simple reaction is now recognized as a complex, high-temperature, short-time heterogeneous process limited by gas-phase and solid-state diffusion with simultaneous physical transformations of the solid. The intrinsic sulfation reaction is so rapid that kinetic rate data for the high-temperature reaction are elusive.

Experimental data obtained from laboratory-scale reactors simulating boiler injection conditions are clouded by a host of competing processes. To better understand the relative influence and importance of each of the processes involved in the sulfation of CaO, mathematical models of varying complexity have been developed.

The concept of modeling the CaO structure as overlapping spheres introduced by Lindner and Simonsson (1981) has been applied by Milne et al. (1990) to the sintering of CaO. Milne et al. explained that the modeling of CaO as a matrix of overlapping spherical grains approximates the structure observed in SEM micrographs and accommodates the various physical transformations necessary for modeling the sulfation of dry sorbents injected in utility boilers (calcination, sintering, pore filling, and particle swelling). They simulated the physical transformation of the CaO sintering process by reducing the grain-center spacing of the matrix of overlapping spherical grains. This mechanism results in a simultaneous loss of surface area and porosity, and this mechanism seems to characterize the SO_2–lime reaction at temperatures typical of utility boilers.

The structural properties of CaO strongly influence pore diffusion and product-layer diffusion, the controlling processes in the sulfation of porous CaO. A comprehensive sulfation model must incorporate these physical aspects of the heterogeneous reaction to accurately simulate the complex process of dry sorbent injection. Concepts, not already developed by Milne et al. (1990) for calcination and sintering, necessary to model the sulfation of CaO with the overlapping grain model are detailed hereafter. The sulfation model is designed for combination with the calcination and sintering models developed by Milne et al. to mathematically analyze the sulfation of small $CaCO_3$ or $Ca(OH)_2$ particles injected into the post-flame zone of pulverized coal boilers.

Structure Changes from Sulfation

Figure 1 shows high-resolution SEM photomicrographs of 2.5-μm hydrate particles injected in a 1367 K gas stream, with and without the presence of SO_2. The procedures for producing these samples were outlined by Milne et al. (1990). The solid in Figure 1a is completely calcined, based on the calcination model of Milne et al., and shows the flash-calcined CaO structure without sulfation. The extent of sulfation of the solid in Figure 1b was 0.15 after 0.04 s, based on measured SO_2 capture levels. This sulfated CaO shows a dramatic reduction in surface texture, indicating a loss of surface area and porosity.

The sulfation of porous CaO is limited by diffusional processes that are strongly dependent on the particle structure. SO_2 diffuses through the porous particle and through the product layer of $CaSO_4$ to react with CaO. Because the molar volume of $CaSO_4$ is 2.72 times that of CaO, CaO grains swell from sulfation. As these grains that constitute the porous solid swell, the rate of sulfation is retarded by hindered diffusion from increased product-layer thickness and from reduced porosity.

Often, the molar volume of $CaSO_4$ is reported as 3.09 times that of CaO. This value is correct for temperatures less than 473 K where the low density (2.61 g/cm^3) $CaSO_4$ crystal structure is stable (Weast, 1981; Wenk and Henkels, 1978). For high-temperature sulfation of CaO, the density of the stable form of $CaSO_4$ (2.96 g/cm^3) should be used. CaO has a density of 3.32 g/cm^3 (Weast, 1981).

Due to this increase in molar volume, Hartman and Coughlin (1974) theorized that the maximum extent of sulfation is limited by the available pore volume for product $CaSO_4$. Borgwardt and Harvey (1972) measured a progressive decrease in pore volume for 250-μm CaO particles reacting with SO_2. However, after 50% conversion, which equates to a porosity of 0.05 based on the original CaO porosity of 0.49, a steady increase in particle volume was observed as sulfation continued beyond the theoretical pore volume limit. Extensive sulfation measurements with 1-μm CaO particles by Borgwardt and Bruce (1986) revealed sulfation levels much greater than

* Author to whom all correspondence should be addressed.

0888-5885/90/2629-2192$02.50/0

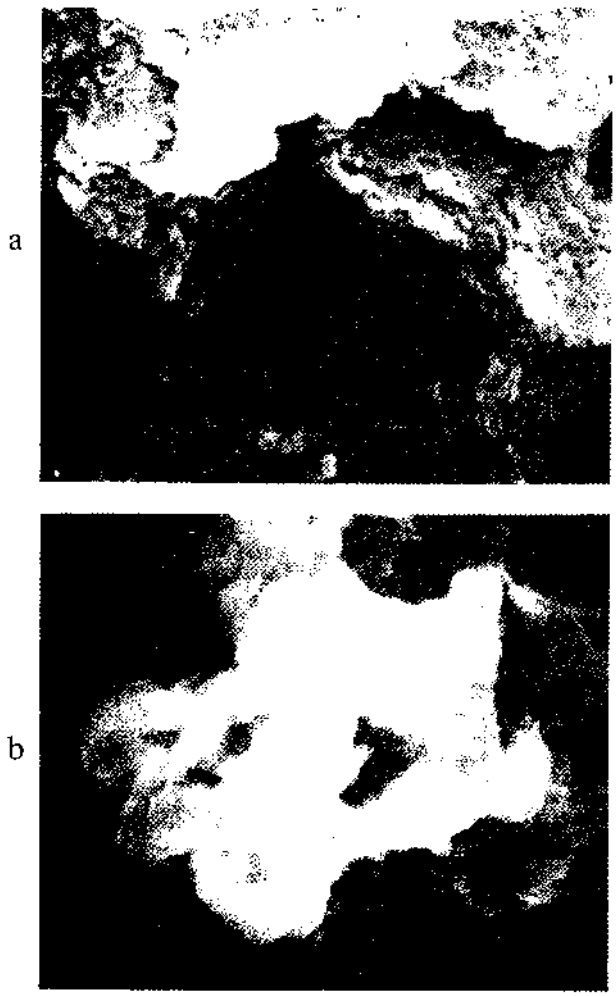

Figure 1. SEM photomicrographs of 2.5-μm-diameter Linwood hydrate 0.04 s after injection in 1367 K gas stream (a) without sulfur dioxide and (b) with sulfur dioxide (2.0 cm = 7.0 μm).

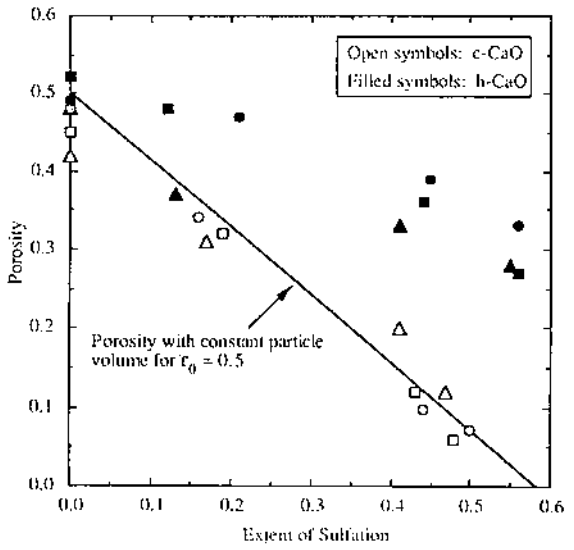

Figure 2. Influence of sulfation on the porosity of <3-μm CaO particles (Gullett and Bruce, 1987). Each symbol corresponds to CaO of a different initial surface area sulfated in a differential fixed-bed reactor.

the theoretical pore volume limit. Sulfation levels in excess of the theoretical pore volume limit can occur only if the particle volume increases.

The data of Gullett and Bruce (1987), plotted in Figure 2, support the contention that CaO particles swell during

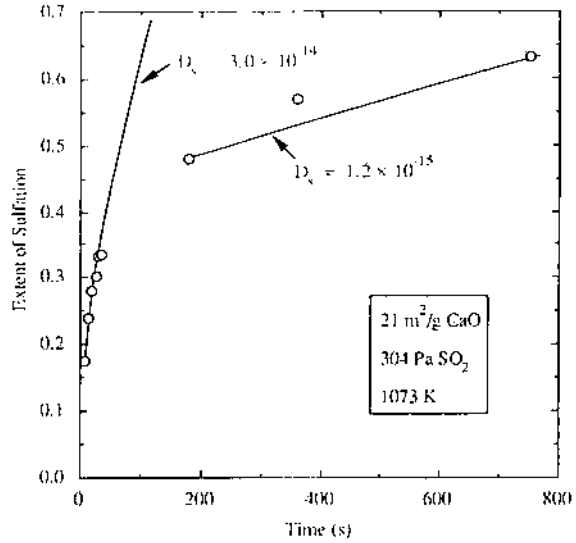

Figure 3. Differential reactor sulfation data of Borgwardt and Bruce (1986) showing the influence of grain isolation (on the apparent product-layer diffusivity).

sulfation. For constant particle volume, the porosity for a given extent of sulfation is given by

$$\epsilon = \epsilon_0 - 1.72(1 - \epsilon_0)x \qquad (2)$$

The line representing this equation in Figure 2, for ϵ_0 = 0.5, shows minor swelling for the carbonate-derived CaO (c-CaO); however, significant deviation from the slope of eq 2 for the hydrate-derived CaO (h-CaO) indicates substantial particle swelling. On the average, the data suggest an 11% particle volume expansion for c-CaO and 40% for h-CaO. As with sintering, the tendency for the porous particle to swell might be enhanced at higher temperatures. It is uncertain whether this propensity at 1073 K for h-CaO to swell more than c-CaO persists at temperatures of interest for upper-furnace injection (>1300 K).

Gullett and Bruce also reported a slight upward shift in the mean pore diameter of the pore size distribution plots for sulfated CaO. This preferential filling of smaller pores suggests that swelling may not be uniform throughout the particle. The sulfation data of Borgwardt and Bruce (1986) not only support the notion of particle swelling but also show evidence of pore filling and the associated isolation of CaO grains. Grain isolation from pore filling could explain the fact that the time-resolved sulfation data of Figure 3 yield radically different product-layer diffusivities when the slope of the data for different time regimes is used to determine the value of the diffusivity. The reduced value is probably due to selective pore closure and grain isolation rather than an actual decrease in the value of the product-layer diffusivity.

The mechanism that preserves some pore volume by particle swelling and simultaneously fills other pores with $CaSO_4$ is not understood. Possibly the phenomenon is governed by two competing processes, the dominance of one depending on grain or pore size differences.

As an approximation of the complex process of preferential expansion of the matrix of CaO grains and pore filling, it is assumed that particle swelling does not take place until the sulfated CaO reaches a minimum porosity of 0.02, the lowest measured value for highly sintered CaO. To accommodate sulfation subsequent to the onset of particle swelling, a constant porosity of 0.02 is maintained thereafter. With this approximation, simultaneous swelling and partial pore filling for a single particle can take place is different zones of the solid have different porosities and sulfation rates.

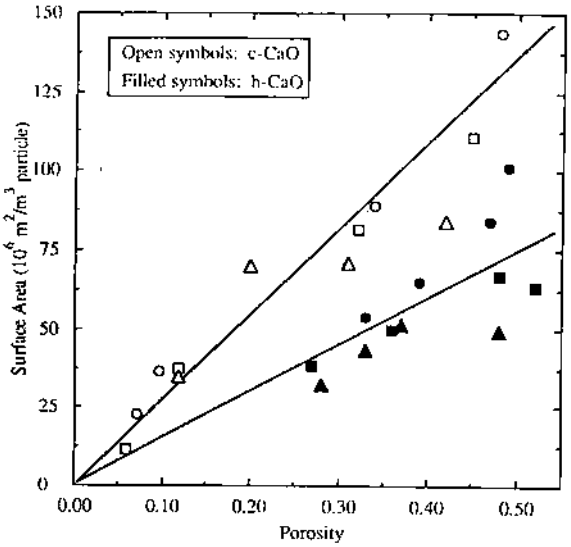

Figure 4. Surface area and porosity data for CaO of differing initial surface areas (represented by different symbols) for various levels of sulfation (Gullett and Bruce, 1987). The far right symbol of each series is the unsulfated CaO.

For sulfation prior to reaching this assumed swelling point, porosity steadily decreases as described by eq 2. To illustrate how the surface area subsequently changes, the data of Gullett and Bruce (1987) are plotted in Figure 4. In general, the surface area per particle volume decreases in direct proportion to the change in porosity induced by sulfation,

$$S_2 = S_1 - (S_1/\epsilon_1)(\epsilon_1 - \epsilon_2) \tag{3}$$

This same relation was observed for the sintering of CaO (Milne et al., 1990).

Because the mean pore diameter is calculated as $4\epsilon/S$ (Smith, 1981), eq 3 results in a constant pore diameter through the sulfation and sintering processes. Pore size distribution plots of Gullett and Bruce (1987) indicated a slight increase in pore diameter during sulfation. The combination of eqs 2 and 3 indicates that small-pore-diameter CaO, steep slope on the Figure 4 plot, loses surface area more rapidly than large-pore CaO for the same extent of sulfation. As a consequence of the strong relationship between surface area and sulfation rate reported by Borgwardt and Bruce (1986), high surface area CaO has a more rapid decline in its rate of sulfation than does low surface area CaO for an equivalent reduction in pore volume.

Overlapping Grain Model

From the development of Milne et al. (1990), the equations governing the surface area and porosity of a particle composed of overlapping spherical CaO grains are (see Figure 5 for a diagram of the grain structure)

$$S = N4\pi^2\left[1 - \frac{n}{2}\left(1 - \frac{r_i}{r}\right)\right] \tag{4}$$

$$1 - \epsilon = N\frac{4}{3}\pi r^3\left\{1 - \frac{n}{4}\left[2 - 3\frac{r_i}{r} + \left(\frac{r_i}{r}\right)^3\right]\right\} \tag{5}$$

$$n = \begin{cases} 12, & \text{for } \epsilon \le 0.26 \\ 27.64\exp(-3.209\epsilon), & \text{for } \epsilon > 0.26 \end{cases} \tag{6}$$

The procedures for obtaining the initial values of N, r, and r_i were described by Milne et al. (1990). The surface area and volume of individual grains are

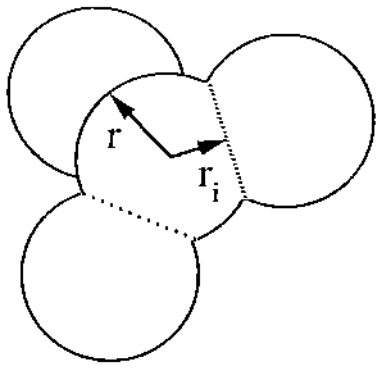

Figure 5. Illustration of the overlapping grain model.

$$S_g = 4\pi^2\left[1 - \frac{n}{2}\left(1 - \frac{r_i}{r}\right)\right] \tag{7}$$

$$V_g = \frac{4}{3}\pi r^3\left\{1 - \frac{n}{4}\left[2 - 3\frac{r_i}{r} + \left(\frac{r_i}{r}\right)^3\right]\right\} \tag{8}$$

The term CaO grain, used in the context of this paper, does not refer to pure crystals of CaO. Rather, it refers to the interconnected solids remaining after calcination of impure limestone or hydrated lime containing non-calcium compounds. This terminology is consistent with the common usage of the terms carbonate and hydrate when referring to the impure stones that are typically only 90–95% pure $CaCO_3$ or $Ca(OH)_2$.

For each time step, structural changes due to sulfation are calculated. The grain volume for a given extent of sulfation is calculated with eq 9

$$V_g = V_{g0}[1 - x + x[v_I + 2.72(1 - v_I)]] \tag{9}$$

which accounts for the presence of inert solids that do not react with SO_2. With a high volume fraction of these inert species, v_I, the grain will expand to a lesser extent with sulfation. As an approximation, the density of the non-CaO species in a CaO sample of known calcium content is assumed to be 2.7 g/cm^3 (density of SiO_2) in order to estimate v_I.

After the increased grain volume is determined with eq 9, the sequence of subsequent calculations depends on whether the particle is at the minimum porosity that initiates particle swelling.

Particle Swelling Solution Scheme. Particle swelling is treated in a manner opposite to that of particle shrinkage from sintering. To account for increased particle volume, the distance between overlapping grain centers, $2r_i$, is increased. For particle swelling $\epsilon = 0.02$, the number density of grains decreases upon sulfation, $N = (1 - \epsilon)/V_g$, due to the increased grain volume, eq 9. The value of n is obtained with eq 6. As $\epsilon \to 0$, $S \to 0$, so r_i/r has a minimum value of $1 - 2/n$. To maintain consistency with this fact, the relation $r_i/r = 0.8333 + 0.6026\epsilon$ is employed (Milne et al., 1990). With this value of r_i/r, eq 8 is solved explicitly for r, which in turn is used to find r_i. Equation 4 yields the value of S.

Pore-Filling Solution Scheme. Where sulfation results in the loss of pore volume without particle expansion, the number density of grains, N, remains unchanged by sulfation. After each sulfation time step, V_g, from eq 9, is used to calculate the reduced porosity, $\epsilon = 1 - NV_g$. Equation 3 subsequently yields a value for S. After evaluating n with eq 6, the nonlinear surface area and

porosity equations for overlapping spheres, eqs 4 and 5, are solved for r and r_i by the Newton–Raphson method.

The physical transformations simulated by the overlapping grain model have a strong influence on the process of product-layer diffusion, which is subsequently demonstrated.

Product-Layer Diffusion

Borgwardt et al. (1987) contended that the diffusion of SO_2 through the $CaSO_4$ product layer to react with CaO is a solid-state mechanism rather than a gas-phase transport. Because the actual mechanism for transport through the product layer is not fully understood, the hypothesis of solid-state diffusion is adopted for this study.

A simplified mechanism, analogous to that described by Silcox et al. (1987), that describes such transport is (1) reversible adsorption and oxidation of SO_2 and O_2 on the $CaSO_4$ surface, (2) diffusion of surface adsorbed SO_3 to subsurface SO_3 vacancies, (3) vacancy jump diffusion of SO_3 through the $CaSO_4$ solid, and (4) sulfation of CaO by reversible exchange of SO_3 between $CaSO_4$ and CaO molecules at the $CaSO_4$/CaO interface. Thus, rather than a single SO_3 molecule diffusing through the entire product layer, transport could take place by a vacancy jump method (Fredericks, 1975). This mechanism describes the net effect of a more complex transport process. For this study, it is assumed that the diffusion steps limit the local rate of reaction at the grain level, so steps 1 and 4 are at equilibrium. Because O_2 concentrations in the gas phase are typically an order of magnitude higher than SO_2 concentrations, the O_2 concentration is essentially constant throughout the reaction and is therefore included in the rate constant.

The solid-state diffusion of SO_3 through the $CaSO_4$ product layer of a spherical grain of CaO is governed by the differential equation

$$\frac{\mathrm{d}}{\mathrm{d}r}\left(S_r \frac{\mathrm{d}c}{\mathrm{d}r}\right) = 0 \tag{10}$$

when the pseudo-steady-state approximation is employed and constant product-layer diffusivity is assumed. Bischoff (1963) and Luss (1968) showed the validity of this approximation when applied to gas–solid reactions. For a sphere, $S_r = 4\pi r^2$. For an overlapping sphere, eq 7 is employed to account for the fact that the entire surface area of the sphere is not in contact with the gas phase. Equation 10 is based on the assumption of spherical symmetry, so its application to an overlapping sphere is an approximation of the slightly asymmetric solid-state diffusion.

For this study, sulfation of an exposed CaO surface is assumed to be instantaneous, limited only by gas-phase diffusion to the surface. This approximation of rapid initial sulfation is supported by measurements in a dispersed-phase reactor at 1367 K that revealed 16% conversion of 2.5-μm h-CaO (Linwood base) within 0.04 s of injection (Milne, 1988).

After a monolayer of $CaSO_4$ molecules has covered the CaO surface, approximately 4-Å thick, it is assumed that the local rate of sulfation at the grain level is limited by diffusion of SO_3 through the product layer. Consequently, the boundary conditions for eq 10 are

$$\text{at } r = r_c, \qquad g = -S_c D_s' \frac{\mathrm{d}c}{\mathrm{d}r} \tag{11}$$

$$\text{at } r = r_s, \qquad c = c_s \tag{12}$$

The term g is the SO_2 generation for a single grain. For SO_2 consumption, g is negative. Integration of eq 10 with these boundary conditions yields

$$c_s - c_c = -\frac{g}{D_s'} \int_{r_c}^{r_i} \frac{\mathrm{d}r}{S_r} \tag{13}$$

If $r_c \geq r_i$, eq 7 is substituted for S_r to complete the integration. If $r_c < r_i$, eq 13 is treated as the sum of two integrals: for $r < r_i$, $S_r = 4\pi r^2$, and for $r \geq r_i$, eq 7 is substituted for S_r. The equilibrium concentration at the CaO interface c_c, is assumed to be approximately zero.

Because the adsorption/oxidation reaction is fast relative to the product-layer diffusion, the solid-phase surface concentration, c_s, is assumed to be at equilibrium with the gas-phase concentration,

$$c_s = K_s(c_{SO_2} - c_e)^m \tag{14}$$

This expression accounts for a nonlinear concentration dependence observed by Borgwardt and Bruce (1986). The Langmuir–Hinshelwood formulation (Smith, 1981) is preferred for adsorption/surface reactions but such a treatment here renders the subsequent mathematics unmanageable. Furthermore, data are not available to specify the multiple parameters of a Langmuir–Hinshelwood expression.

The finite vapor pressure of SO_2 above solid $CaSO_4$ is accounted for by c_e. Reid (1970) reported values of the equilibrium constant for the sulfation reaction, eq 1, from which c_e is evaluated,

$$c_e = \left[9.875 \times 10^{-17} \exp\left(\frac{54540}{T}\right) T p_{O_2}^{1/2}\right]^{-1} \tag{15}$$

Values calculated from eq 15 are comparable to the experimental data plotted by Bortz and Flament (1985).

With these approximations and the relation $D_s = K_s D_s'$, integration of eq 13 results in the rate expression

$$-G = \frac{N 4\pi D_s (c_{SO_2} - c_e)^m}{\frac{-2}{n r_i} \ln\left[1 - \frac{n}{2}\left(1 - \frac{r_i}{r_s}\right)\right] + \theta}$$

$$\theta = \begin{cases} \dfrac{2}{n r_i} \ln\left[1 - \dfrac{n}{2}\left(1 - \dfrac{r_i}{r_c}\right)\right], & \text{for } r_c \geq r_i \\ \dfrac{1}{r_c} - \dfrac{1}{r_i}, & \text{for } r_c < r_i \end{cases} \tag{16}$$

The term G is the rate of generation of SO_2 per particle volume. Equation 16 is applicable after complete monolayer coverage of the grain with $CaSO_4$, thus avoiding the discontinuity at $r_c = r_s$.

Equation 16 is used to determine the moles of CaO sulfated for a small time step. The resultant increase in grain volume and product-layer thickness necessitates changes in the structural parameters of the overlapping grains, which influence subsequent rate values determined with eq 16. The reaction is assumed to be irreversible for the model calculations.

As the value of r_i approaches that of r_s, eq 16 reduces to the form of the equation of a nonoverlapping sphere. Grain overlap reduces the rate of product-layer diffusion by accounting for limited surface area for diffusion relative to a single sphere. In addition, the limited surface area results in a thicker product layer for a given extent of sulfation. Figure 6 illustrates this hindrance due to overlap. As the degree of overlap or the coordination number increases, the denominator of eq 16 increases in value over that of a simple sphere, thus reducing the rate

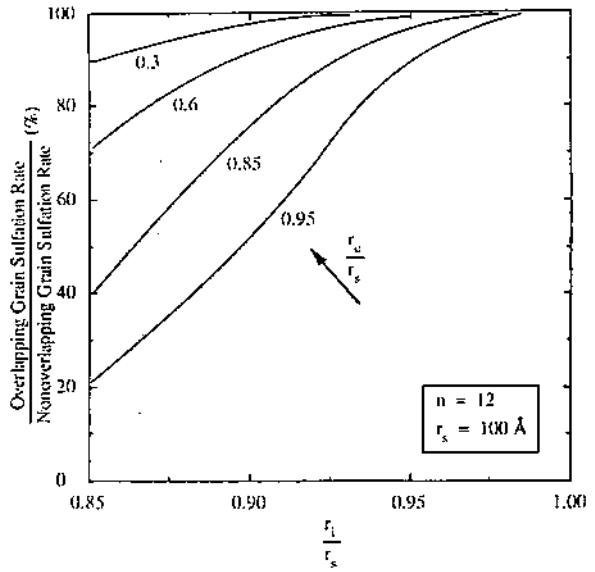

Figure 6. Comparison of sulfation rates of equal diameter (200-Å) overlapping and nonoverlapping grains.

Table I. Estimated CaO Porosity for the Sulfation Data of Borgwardt and Bruce (1986)

S_m, m²/g	ϵ	S_m, m²/g	ϵ
2.1	0.024	21	0.20
3	0.034	25	0.23
11.5	0.12	35	0.29
15.5	0.15	63	0.43
17	0.17		

of reaction relative to that calculated for a nonoverlapping sphere with the same diameter and product-layer thickness. The difference between the nonoverlapping and overlapping grain models is most significant during the initial stages of sulfation, small r_c/r_s.

Fundamental data for evaluating the rate of product-layer diffusion were reported by Borgwardt and Bruce (1986) and Borgwardt et al. (1987). These data were obtained from differential fixed-bed reactor experiments. CaO particles were prepared by calcination of 1-μm $CaCO_3$ particles in one reactor with variable sintering times to provide a range of surface areas.

To evaluate D_s from these data, it was assumed that pore diffusion is negligible for these 1-μm particles after the first point of the data set, conversion levels being higher than 5%. Subsequent calculations accounting for pore diffusion reveal that, by the time of the first point of each data set, the concentration at the center of the particle was less than 1% different than the bulk gas concentration. To avoid the initial reaction complications involving simultaneous pore diffusion and intrinsically limited sulfation, D_s was obtained by using the first point of each data set as the beginning point for fitting the data with eq 16. As indicated by Figure 3, the earliest data points of each set were evaluated to avoid the complication of preferential grain isolation that results in artificially low values of D_s. Most of the data of Borgwardt and Bruce (1986) are in the particle swelling domain.

Analysis of subsequent CaO data (Milne et al., 1990) obtained from the same reactor provides an estimate of porosity (Table I) associated with the reported surface areas of Borgwardt and Bruce. Porosity is an essential parameter for initializing the overlapping grain model.

Figure 7 examines the influence of gas-phase SO_2 concentration on the product-layer diffusion rate. The nonlinear SO_2 concentration dependence (m = 0.6) is in agreement with the findings of Borgwardt and Bruce

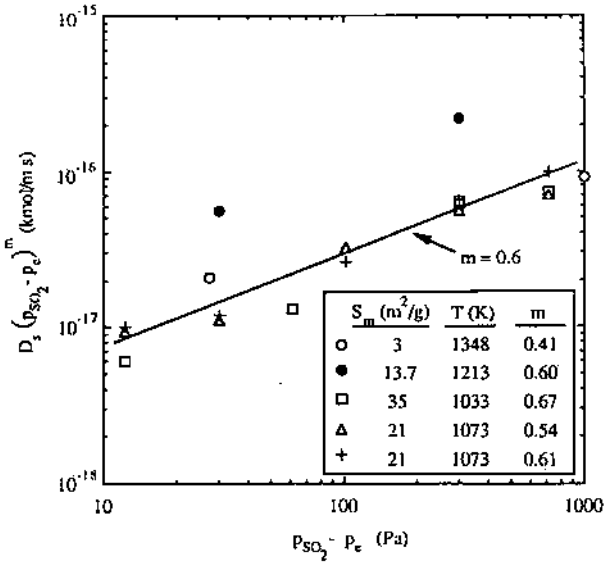

Figure 7. Influence of partial pressure on rate of product-layer diffusion for the data of Borgwardt and Bruce (1986).

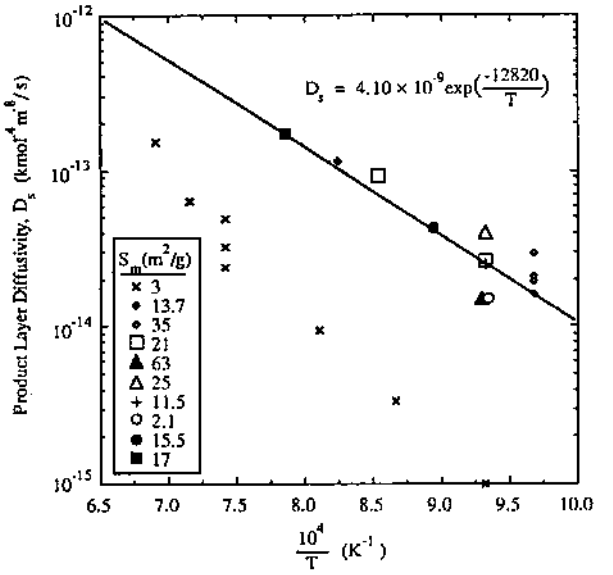

Figure 8. Product-layer diffusion rate constant determined from the data of Borgwardt and Bruce (1986) for CaO of differing surface areas.

(1986) (m = 0.62), Borgwardt et al. (1987) (m = 0.64), and Silcox et al. (1987) (m = 0.55).

With m = 0.6 for eq 16, values of D_s for the data sets of Borgwardt and Bruce are plotted against temperature in Figure 8. To avoid congestion of the plot, the 21 m²/g point at 1073 K represents the average of 11 separate data sets. The 3 m²/g data have a much lower D_s than the rest of the data, apparently because isolation of interior grains occurs at lower conversion levels for the low porosity CaO. The 2.1 m²/g data have much shorter time measurements than the 3 m²/g data. For the long time 2.1 m²/g data, a similar low value of D_s was calculated. However, the short time 2.1 m²/g data, Figure 8, have a D_s value consistent with the higher surface area data. For that reason, the 3 m²/g data were not included in the statistical fit to obtain an equation for D_s,

$$D_s = 4.10 \times 10^{-9} \exp(-12820/T) \qquad (17)$$

In summary, this product-layer diffusivity was arrived at by determining the best fit to the sulfation data of Borgwardt and Bruce (1986) after more than one mono-

layers of $CaSO_4$ molecules covered the CaO grains.

Figure 6 shows how the overlapping grain concept results in lower product-layer diffusion rates than would be calculated with a simple grain model. As a result, the value of the product-layer diffusivity determined by fitting the data with the overlapping grain model is higher than that determined by using a simple grain model.

The overlapping grain concept lends additional insight to the possible structure of low surface area CaO. On the basis of fact that a 1-μm sphere has an external surface area of 1.8 m^2/g, one might expect that the 2.1 and 3 m^2/g CaO represent solid particles on which essentially all sulfation occurs externally. However, internal porosity for low surface area calcines has been observed by nitrogen adsorption methods and by SEM techniques (Milne et al., 1990). A simple grain model is inadequate for explaining low surface area with finite internal porosity. However, the overlapping grain model represents 3 m^2/g CaO with a 0.034 porosity as a matrix of 0.09-μm-diameter overlapping grains with $r_i/r = 0.8538$ [see Milne et al. (1990) for the calculation procedures]. As a result, a 1-μm CaO particle is composed of nearly 1600 of these overlapping grains, showing a significant number of internal sites for sulfation that the simple grain model cannot simulate.

External Mass Transfer

Of significance for large particles or for initially rapid sulfation rates is the rate of transport of SO_2 from the bulk gas phase to the surface of the CaO particle. At low particle Reynolds numbers (low gas velocity or small diameter), the mass-transfer coefficient for a sphere in a gas stream is calculated by using a Sherwood number of 2 (Treybal, 1968). The value of 2 is obtained by deriving the mass-transfer coefficient for a sphere in stagnant gas. Uncertainty as to the effect of potentially high mass-transfer rates for the reaction of SO_2 with a decomposing $CaCO_3$ or $Ca(OH)_2$ particle necessitates inclusion of the bulk flow contributions in the external mass-transfer calculations.

The film theory development of Bird et al. (1960), accounting for high mass-transfer rates in a multicomponent gas phase, showed the influence of bulk flow, F_t, on the flux of SO_2 to the particle surface, F_p,

$$F_p = k^*\left(1 - \frac{F_t}{F_p}y_p\right)^{-1}(y_p - y_b) \tag{18}$$

From the same development,

$$k^* = k\left(\frac{\phi}{e^\phi - 1}\right) \tag{19}$$

$$\phi = F_t/k \tag{20}$$

and for a Sherwood number of 2,

$$k = \frac{c_t D_m}{r_p} \tag{21}$$

The mass-transfer coefficient, k^*, is independent of the mass-transfer rate, whereas k is a function of mass-transfer rate and reduces to k^* in the limit of no mass transfer. Consolidation of eqs 18–21 yields

$$F_p = \frac{c_t D_m}{r_p}\left(\frac{\phi}{e^\phi - 1}\right)\left(1 - \frac{F_t}{F_p}y_p\right)^{-1}(y_p - y_b) \tag{22}$$

The first term in parentheses is the correction due to the curvature of the concentration profile, and the second term in parentheses is the bulk flow correction. When bulk flow, F_t, is small, eq 22 reverts to the simple case of using a Sherwood number of 2 to calculate the flux of SO_2. For the model calculations, the value of F_p from the previous time step is used to explicitly calculate the new value of F_p from eq 22. Of course, D_m and c_t are evaluated at the film temperature for nonisothermal conditions.

To account for the influence of the major species of typical combustion gases (CO_2, H_2O, N_2, and O_2), the effective binary diffusivity of SO_2 in a multicomponent gas mixture is (Bird et al., 1960)

$$D_m = \frac{F_{SO_2} - y_{SO_2}F_t}{\sum_i \frac{1}{D_{SO_2 i}}(y_i F_{SO_2} - y_{SO_2}F_i)} \tag{23}$$

For model calculations, the previous time step values of F_{SO_2} and F_t are used to evaluate eq 23 explicitly.

The Chapman–Enskog formula (Smith, 1981) is used to evaluate the binary diffusivity of SO_2 in each of the combustion gases,

$$D_{SO_2 i} = 0.018829\frac{T^{3/2}\left(\frac{1}{64.07} + \frac{1}{M_i}\right)^{1/2}}{p_t \sigma_{SO_2 i}^2 \Omega_{SO_2 i}} \tag{24}$$

$$\sigma_{SO_2 i} = \frac{1}{2}(4.29 + \sigma_i) \tag{25}$$

$$\Omega_{SO_2 i} = 1.121 - 0.07921\gamma + 0.005459\gamma^2 - 0.0001320\gamma^3, \quad \text{for } 4 < \gamma < 20 \tag{26}$$

where $\gamma = T[252(\epsilon/k)_i]^{-1/2}$. The Lennard-Jones constants are listed in Table II. Equation 26 is a statistical fit of the collision integral values tabulated in Smith (1981).

Table II. Lennard-Jones Parameters[a]

gas (i)	M_i	σ_i, Å	$(\epsilon/k)_i$, K
SO_2	64.07	4.290	252
CO_2	44.01	3.996	190
H_2O	18.02	2.655	363
N_2	28.02	3.681	91.5
O_2	32.00	3.433	113

[a] Smith, 1981; Gambill, 1973.

Effective Pore Diffusivity

A primary element for modeling the simultaneous diffusion and reaction of SO_2 in porous CaO is the effective diffusivity. The molar flux of SO_2 diffusing through porous CaO is proportional to the concentration gradient and the effective diffusivity (Smith, 1981),

$$D_e = \frac{\epsilon}{\tau}\left(\frac{1}{D_m} + \frac{1}{D_K}\right)^{-1} \tag{27}$$

where

$$D_K = 97a(T/64.07)^{1/2} \tag{28}$$

Knudsen diffusivity is directly proportional to the pore radius, a. Bulk diffusion, D_m, predominates in pores of a diameter larger than the mean free path of SO_2 molecules (2200 Å at 1350 K), and Knudsen diffusion, D_K, is the controlling transport mechanism for smaller pores. For sulfation of porous CaO, Knudsen diffusion is the primary mechanism for gas-phase diffusion of SO_2. Therefore, a more rigorous form of eq 27 that includes the bulk flow effects is avoided without loss of accuracy.

Huizenga and Smith (1986) measured Knudsen diffusion in pellets composed of uniform spheres. They showed that Knudsen diffusivities calculated with a mean pore radius

from the relation $a = 2\epsilon/S$ matched their experimental data. Because the uniform packing of spheres used by Huizenga and Smith (1986) approximates the physical characteristics of the overlapping grain model, both in size and shape, the relation $a = 2\epsilon/S$ is used to evaluate the mean pore radius for eq 28, and the tortuosity factor is assumed to be 1.47.

Pore Diffusion

A dominant factor in retarding the rate of sulfation of porous CaO is the limited transport of SO_2 to the interior of the particle. Employing the pseudo-steady-state approximation, the mole balance for SO_2 simultaneously diffusing and reacting through a porous CaO sphere is

$$\frac{d}{dr}\left(D_e r^2 \frac{dc}{dr}\right) + Gr^2 = 0 \tag{29}$$

Integration of this equation is complicated by the nonlinear dependence of G on concentration (see eq 16) and the variation of D_e with radius.

Most sulfation models that include pore diffusion assume first-order concentration dependence to avoid this nonlinearity (Simons and Garman, 1986; Ramachandran and Smith, 1977; Hartman and Coughlin, 1976; Christman and Edgar, 1983; Bhatia and Perlmutter, 1981; Newton, 1987; Lindgren, 1988). Jayaraman et al. (1983) proposed a method of solving the nonlinear differential equation without the complication of changing structure. Silcox (1985) solved this nonlinear differential equation by a finite difference approach that required solution of a nonlinear system of equations by the Newton–Raphson method.

A solution scheme, similar to that employed by Silcox et al. (1989) for the calcination of $CaCO_3$ with CO_2 diffusion limitations (without the generation term of eq 29), was developed to solve eq 29. To calculate the concentration profile through porous CaO, the particle is subdivided into spherical shells, each of which is assumed to have constant D_e and G. The term G is evaluated by using the average value of c_1 and c_2, the boundary concentrations of the shell. For small Δr, this linear average is a reasonable approximation to the true mean value of the nonlinear concentration profile through each shell and leads to a simpler mathematical solution.

The change in concentration through a shell is obtained by integrating eq 29 with boundary conditions

$$\text{at } r = r_1, \qquad c = c_1 \qquad dc/dr = -F/D_e \tag{30}$$

where F is the molar flux of SO_2 at r_1, c_2 is the concentration at r_2, and $r_1 < r_2$:

$$c_2 - c_1 = \frac{G}{D_e}\left[-\frac{1}{6}(r_2^2 - r_1^2) + \frac{r_1^2}{3}\left(1 - \frac{r_1}{r_2}\right)\right] - \frac{Fr_1^2}{D_e}\left(\frac{1}{r_1} - \frac{1}{r_2}\right) \tag{31}$$

Because SO_2 is diffusing into the sphere and converting to solid $CaSO_4$, both G and F are negative. Equation 31 is composed of two generation terms and a single flux term that allow comparison with equations derived from simpler diffusion conditions. The left generation term (involving $r_2^2 - r_1^2$) arises from the case of uniform G throughout the particle, not just the single shell. The second generation term (involving $1 - r_1/r_2$) combined with the flux term reduces the Δc calculated from the first term alone, to account for the fact that G is a function of the SO_2 concentration (the value of G decreases toward the center of the particle). The very right-hand term (the flux term) of the equation is the Δc for the case of no SO_2 consumption through the shell.

A mole balance for diffusion of SO_2 from the bulk gas phase to the particle surface shows

$$F_p = k_m(c_p - c_b) \tag{32}$$

To solve for the concentration profile, the particle is subdivided into $p - 1$ spherical shells of equal volume. The concept of equal shell volumes reduces computer storage requirements and produces a more uniform availability of CaO shells for sulfation as calcination proceeds by the shrinking-core mechanism. Each shell is designated by the same node number, j, as the inside radius of that shell. Node 1 is the center of the spherical particle, and node p is the surface of the particle. It is important to note that for shell j

$$F_j r_j^2 = \sum_{i=1}^{j-1} \frac{G_i}{3}(r_{i+1}^3 - r_i^3), \quad \text{for } j > 1 \tag{33}$$

Obviously, $F_1 r_1^2 = 0$. Given the value of D_e for each shell, the bulk gas concentration of SO_2, c_b, and an initial estimate of the concentration at each node or the previous time step concentrations, the values of G_j and F_j are calculated for each node by using eqs 16 and 33. Equation 32 is solved to obtain c_p, and eq 31 is applied to each of the subsequent shells.

Iteration of this procedure with direct substitution of the most recent mean shell concentrations converges rapidly if the mean shell concentrations toward the center of the particle do not approach c_e. To provide stable convergence of the concentration profile in all cases, the estimate of the mean shell concentration is updated after each iteration by taking the square root of the product of the newly calculated value and the estimated value used in the previous calculation.

Model Comparison to Data

To evaluate the sulfation model (combined effects of external mass transfer, pore diffusion, and product-layer diffusion), model predictions were compared with the data of Borgwardt and Bruce (1986). It must be kept in mind that these data were previously used to evaluate the product-layer diffusivity only. Early stage sulfation, where gas-phase mass-transfer limitations are significant, was avoided in the determination of the values of D_e.

Figure 9 compares model predictions with sulfation data obtained at various SO_2 partial pressures. The model agrees reasonably well with the data in terms of both position on the plot and shape of the curve.

Figure 10 is a comparison of the model predictions for CaO of differing surface areas. The porosities listed in Table I are employed by the model for these predictions. The disparity between predicted and actual values for 63 m^2/g could result from sintering. The sintering data of Borgwardt (1989) for CaO in a nitrogen atmosphere indicate that sintering of the 63 m^2/g CaO for 1073 K in less than 40 s is negligible, but Newton (1987) proposed that SO_2 catalyzes sintering in a manner similar to that of CO_2 and H_2O. For the lower surface area calcines, the model predicts much less difference between the sulfation rates of the 21 and 25 m^2/g CaO than the data show.

Model predictions of Figure 11 indicate the same trend of underpredicting the sulfation level of 21 m^2/g CaO, even at the higher temperature of 1173 K. However, the Figure 11 predictions for 35 m^2/g CaO at 1033 K show better agreement with the data. Thus, the model predicts the general trends of the surface area data without a consistent deviation over the range of surface areas. The random deviation between theoretical and actual values at higher surface areas could be partially due to error in the esti-

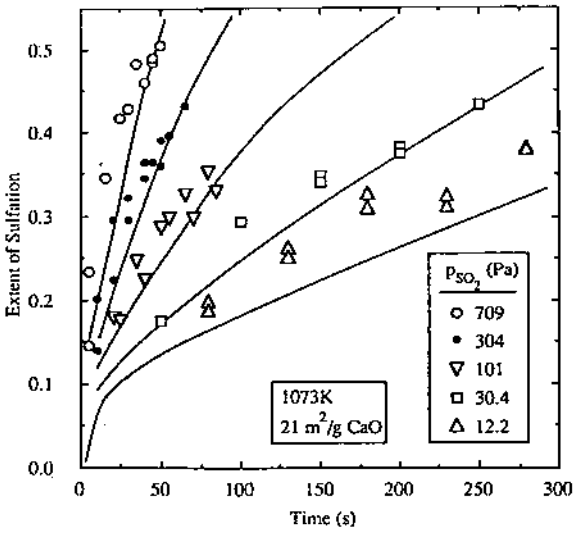

Figure 9. Model predictions of the influence of partial pressure compared to the sulfation data of Borgwardt and Bruce (1986) for CaO derived from Georgia Mable and Vicron limestones.

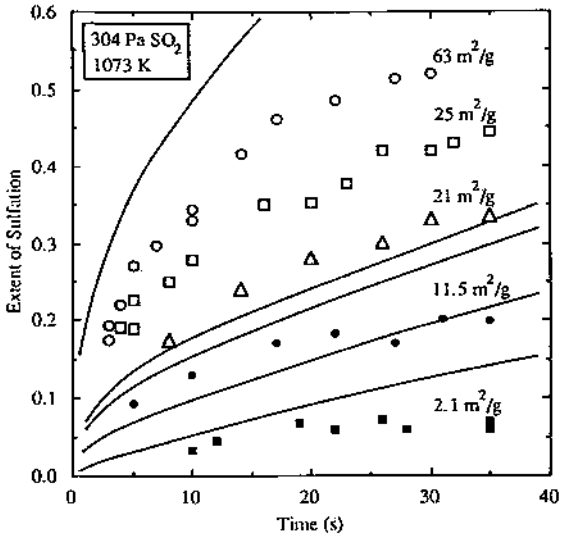

Figure 10. Model predictions for different surface area CaO compared with sulfation data of Borgwardt and Bruce (1986) for 1-μm CaO derived from Fredonia limestone.

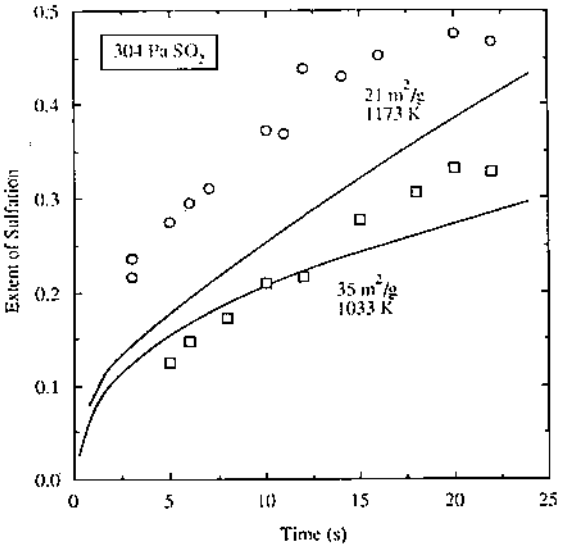

Figure 11. Model predictions for different surface areas and temperatures compared with the data of Borgwardt and Bruce (1986) for 1-μm CaO derived with Fredonia limestone.

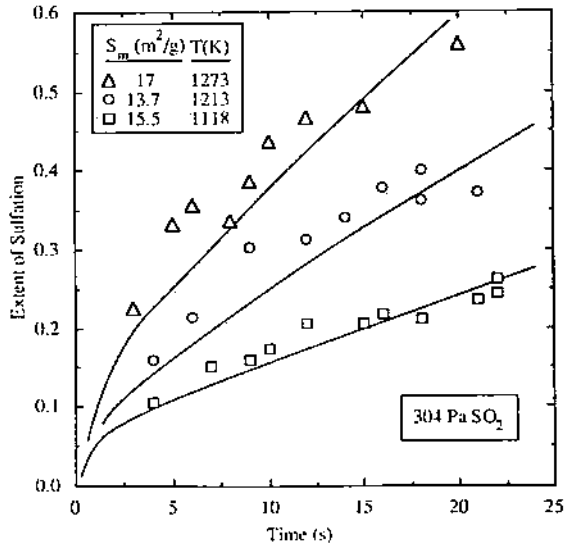

Figure 12. Model prediction of temperature influence compared to sulfation data (Borgwardt and Bruce, 1986) for 1-μm CaO with similar surface areas derived from Fredonia limestone.

mates of the CaO porosities. This random deviation also suggests that experimental error is probably magnified when measuring with the more reactive high surface area calcines.

Figure 12 illustrates the influence of temperature on the rate of sulfation for three calcines of similar surface area. In this case, the agreement between model predictions and experimental data is quite good.

Conclusions

The overlapping grain model developed for the sintering of CaO (Milne et al., 1990) is readily adapated to stimulate physical transformations for the sulfation of porous CaO. The model accounts for the sulfation induced loss of surface area and porosity and the resultant reduction in reactivity. Simultaneous sintering of high surface area CaO during sulfation retards the rate of product-layer diffusion by moving adjacent grains closer together, resulting in a diminished grain surface area for diffusion.

It is assumed that particle swelling commences at 0.02 porosity to maintain constant porosity through subsequent sulfation. Prior to particle swelling, sulfation occurs with a constant particle volume, resulting in a loss of porosity from the swelling of the sulfated CaO grains. The model can accommodate the simultaneous particle swelling and pore filling observed experimentally, but a fundamental understanding of the competing transformation is lacking.

Sulfation of the exposed CaO surface is assumed to be instantaneous, limited only by gas-phase diffusion, until a monolayer of $CaSO_4$ molecules covers the surface. The intrinsic rate for this extremely rapid reaction is not clearly defined by the limited body of fundamental short-time sulfation data. Subsequent to monolayer coverage, the sulfation rate is controlled by combined pore-diffusion and product-layer diffusion. The equations necessary to model gas-phase diffusion are developed but not thoroughly tested with experimental data in this portion of the paper. Such discussion is the subject of part 2 of this paper.

The latter stages of sulfation of small CaO particles are dominated by product-layer diffusion. The product-layer diffusivity was determined from sulfation data of 1-μm CaO particles where the reaction was limited entirely by product-layer diffusion (Borgwardt and Bruce, 1986). The complex mechanism of SO_2 reacting with a CaO grain covered with a layer of $CaSO_4$ is modeled with a global

order of 0.6. As a consequence, pore diffusion is represented with a nonlinear differential equation, the numerical solution of which was developed for this study. Excess O_2 allows assumption of an effective zero-order O_2 concentration dependence for atmospheres typical of those experienced in sorbent injection.

The sulfation model, including monolayer sulfation and gas-phase and product-layer diffusion, shows acceptable agreement with the early time scale differential reactor data of Borgwardt and Bruce and not just the period of product-layer diffusion control where the model was fit to the data. This development of the sulfation model based on relatively low-temperature data provides a basis for investigating sulfation rates at sorbent injection times (<1 s) and temperatures (>1300 K).

Acknowledgment

We gratefully acknowledge the U.S. EPA's extensive financial support and continuing technical assistance throughout the project. This work was also sponsored in part by the Advanced Combustion Engineering Research Center. Funds for this Center are received from the National Science Foundation, the State of Utah, 25 industrial participants, and the U.S. Department of Energy.

Nomenclature

a = pore radius (m)
c = gas-phase concentration of SO_2 or solid-phase concentration of SO_3 (kmol/m^3)
c_b = bulk gas-phase concentration of SO_2 (kmol/m^3)
c_c = solid-phase concentration of SO_3 at the $CaO/CaSO_4$ interface (kmol/m^3)
c_e = equilibrium gas-phase concentration of SO_2 (kmol/m^3)
c_p = gas-phase concentration of SO_2 at the particle surface (kmol/m^3)
c_s = solid-phase concentration of SO_3 at the grain surface (kmol/m^3)
c_{SO_2} = gas-phase concentration of SO_2 (kmol/m^3)
c_t = total gas-phase concentration (kmol/m^3)
D_e = effective gas-phase pore diffusivity of SO_2 (m^2/s)
D_K = Knudsen diffusivity of SO_2 (m^2/s)
D_m = effective gas-phase binary diffusivity of SO_2 in a gas mixture (m^2/s)
D_s = product-layer diffusivity in terms of gas-phase SO_2 concentration (kmol$^{0.4}$ m$^{0.8}$/s)
D_s' = product-layer diffusivity in terms of solid-phase SO_3 concentration (m^2/s)
D_{SO_2i} = binary diffusivity of SO_2 in a mixture of SO_2 and gas species i (m^2/s)
F = molar flux of SO_2 (kmol/(m^2 s))
F_i = molar flux of gas species i at the particle surface or molar flux of gas-phase SO_2 at the inside radius of shell i (kmol/(m^2 s))
F_p = molar flux of gas-phase SO_2 at the particle surface (kmol/(m^2 s))
F_t = total molar flux of all gas species at the particle surface (kmol/(m^2 s))
g = generation of SO_2 from a single CaO grain (kmol/s)
G = generation of SO_2 per particle volume (kmol/(m^3 s))
G_i = generation of SO_2 per particle volume in shell i (kmol/(m^3 s))
k = mass-transfer coefficient uncorrected for finite mass transfer (kmol/(m^2 s))
k^* = mass-transfer coefficient corrected for finite mass transfer (kmol/(m^2 s))
k_m = external mass-transfer coefficient (m/s)
K_s = equilibrium constant for adsorption/oxidation of SO_2 on $CaSO_4$ (kmol$^{0.4}$/m$^{1.2}$)
m = effective reaction order
M_i = molecular weight of species i
n = coordination number
N = CaO grain number density (m^{-3})
p_i = partial pressure of gas i (Pa)
p_e = equilibrium partial pressure of SO_2 (Pa)
p_t = total pressure (Pa)
r = CaO grain radius (m)
r_c = unreacted CaO core radius (m)
r_i = radius for interface with neighbor overlapping sphere (m)
r_p = particle radius (m)
r_s = outside grain radius (m)
S = surface area per particle volume (m^{-1})
S_c = unreacted CaO core surface area (m^2)
S_g = surface area of overlapping grain (m^2)
S_m = specific surface area (m^2/g)
S_r = diffusion area at radius r (m^2)
t = time (s)
T = temperature (K)
v_I = volume fraction of inert solids in the CaO
V_g = volume of overlapping grain (m^3)
V_{g0} = initial volume of unsulfated grain (m^3)
y_i = gas-phase mole fraction of species i
y_b = mole fraction of SO_2 in the bulk gas phase
y_p = gas-phase mole fraction of SO_2 at the particle surface
x = extent of sulfation

Greek Letters

γ = parameter defined in eq 26
ϵ = porosity (void fraction)
ϵ_0 = initial porosity
$(\epsilon/k)_i$ = Lennard-Jones parameter related to potential energy (K)
θ = term defined in eq 16
σ_{SO_2i} = Lennard-Jones collision diameter for a mixture of SO_2 and species i (Å)
τ = tortuosity factor
ϕ = dimensionless term defined by eq 20
Ω_{SO_2i} = dimensionless collison integral for SO_2 in a mixture of SO_2 and species i

Registry No. CaO, 1305-78-8; $CaCO_3$, 471-34-1; $Ca(OH)_2$, 1305-62-0; SO_2, 7446-09-5.

Literature Cited

Bhatia, S. K.; Perlmutter, D. D. A Random Pore Model for Fluid-Solid Reactions: II. Diffusion and Transport Effects. *AIChE J.* **1981**, *27*, 247.

Bird, R. B.; Stewart, W. E.; Lightfoot, E. N. *Transport Phenomena*; Wiley: New York, 1960.

Bischoff, K. B. Accuracy of the Pseudo Steady State Approximation for Moving Boundary Diffusion Problems. *Chem. Eng. Sci.* **1963**, *18*, 711.

Borgwardt, R. H. Sintering of Nascent Calcium Oxide. *Chem. Eng. Sci.* **1989**, *44*, 1.

Borgwardt, R. H.; Bruce, K. R. Effect of Specific Surface Area on the Reactivity of CaO with SO_2. *AIChE J.* **1986**, *32*, 239.

Borgwardt, R. H.; Harvey, R. D. Properties of Carbonate Rocks Related to SO_2 Reactivity. *Environ. Sci. Technol.* **1972**, *6*, 350.

Borgwardt, R. H.; Bruce, K. R.; Blake, J. An Investigation of Product-Layer Diffusivity for CaO Sulfation. *Ind. Eng. Chem. Res.* **1987**, *26*, 1993.

Bortz, S. J.; Flament, P. Recent IFRF Fundamental and Pilot Scale Studies on the Direct Sorbent Injection Process. *Proc. 1st Joint Symp. on Dry SO_2 and Simul. SO_2/NO_x Control Technol.*, EPA-600/9-85-020a (NTIS PB85-232353); EPA: Washington, DC, July 1985; Vol. 1, p 17–1.

Christman, P. G.; Edgar, T. F. Distributed Pore-Size Model for Sulfation of Limestone. *AIChE J.* **1983**, *29*, 388.

Fredericks, W. J. Diffusion in Alkali Halides. In *Diffusion in Solids, Recent Developments*; Nowick, A. S., Burton, J. J., Eds.; Academic: New York, 1975.

Gambill, W. R. Prediction and Correlation of Physical Properties. In *Chemical Engineers' Handbook*, 5th ed.; Perry, R. H., Chilton, C. H., Eds.; McGraw-Hill: New York, 1973.

Gullett, B. K.; Bruce, K. R. Pore Distribution Changes of Calcium-Based Sorbents Reacting with Sulfur Dioxide. *AIChE J.* **1987**, *33*, 1719.

Hartman, M.; Coughlin, R. W. Reaction of Sulfur Dioxide with Limestone and the Influence of Pore Structure. *Ind. Eng. Chem. Process Des. Dev.* 1974, *13*, 248.

Hartman, M.; Coughlin, R. W. Reaction of Sulfur Dioxide with Limestone and the Grain Model. *AIChE J.* 1976, *22*, 490.

Huizenga, D. G.; Smith, D. M. Knudsen Diffusion in Random Assemblages of Uniform Spheres. *AIChE J.* 1986, *32*, 1.

Jayaraman, V. K.; Kulkarni, B. D.; Doraiswamy, L. K. Simple Method for Solution of a Class of Reaction-Diffusion Problems. *AIChE J.* 1983, *29*, 521.

Lindgren, E. R. Fuel Rich Sulfur Capture. Ph.D. Dissertation, The University of Utah, Salt Lake City, 1988.

Lindner, B.; Simonsson, D. Comparison of Structural Models for Gas-Solid Reactions in Porous Solids Undergoing Structural Changes. *Chem. Eng. Sci.* 1981, *36*, 1519.

Luss, D. On the Pseudo Steady State Approximation of Gas Solid Reactions. *Can. J. Chem. Eng.* 1968, *46*, 154.

Milne, C. R. High-Temperature, Short-Time Sulfation of Calcium-Based Sorbents. Ph.D. Dissertation, The University of Utah, Salt Lake City, 1988.

Milne, C. R.; Silcox, G. D.; Pershing, D. W.; Kirchgessner, D. A. Calcination and Sintering Models for Application to High-Temperature, Short-Time Sulfation of Calcium-Based Sorbents. *Ind. Eng. Chem. Res.* 1990, *29*, 139–149.

Newton, G. H. Sulfation of Limestone in a Combustion Environment. PhD. Dissertation, The University of Utah, Salt Lake City, 1987.

Ramachandran, P. A.; Smith, J. M. A Single-Pore Model for Gas-Solid Noncatalytic Reactions. *AIChE J.* 1977, *23*, 353.

Reid, W. T. Basic Factors in the Capture of Sulfur Dioxide by Limestone and Dolomite. *J. Eng. Power, Trans. ASME* 1970, Jan.

Silcox, G. D. Analysis of SO_2-Lime Reaction System: Mathematical Modeling and Experimental Studies with Emphasis on Stoker Application. Ph.D. Dissertation, The University of Utah, Salt Lake City, 1985.

Silcox, G. D.; Chen, S. L.; Clark, W. D.; Kramlich, J. C.; LaFond, J. F.; McCarthy, J. M.; Pershing, D. W.; Seeker, W. R. Status and Evaluation of Calcitic SO_2 Capture: Analysis of Facilities Performance. EPA-600/7-87-014 (NTIS PB87-194783); EPA: Washington, DC, May 1987.

Silcox, G. D.; Kramlich, J. C.; Pershing, D. W. A Mathematical Model for the Flash Calcination of Dispersed $CaCO_3$ and $Ca(OH)_2$ Particles. *Ind. Eng. Chem.* 1989, *28*, 155–160.

Simons, G. A.; Garman, A. R. Small Pore Closure and the Deactivation of the Limestone Sulfation Reaction. *AIChE J.* 1986, *32*, 1491.

Smith, J. M. *Chemical Engineering Kinetics*, 3rd, ed.; McGraw-Hill: New York, 1981.

Treybal, R. E. *Mass-Transfer Operations*, 2nd ed.; McGraw-Hill: New York, 1968.

Weast, R. C., Ed. *CRC Handbook of Chemistry and Physics*, 62nd ed.; CRC: Boca Raton, FL, 1981.

Wenk, R. J.; Henkels, P. L. Calcium Sulfate. In *Kirk–Othmer Encyclopedia of Chemical Technology*, 3rd ed.; Grayson, M., Ed.; Wiley: New York, 1978; Vol. 4.

Received for review January 12, 1990
Revised manuscript received May 21, 1990
Accepted July 11, 1990